Asian Journal of Chemistry; Vol. 33, No. 9 (2021), 2212-2218

ASIAN JOURNAL OF CHEMISTRY

https://doi.org/10.14233/ajchem.2021.23282

Tin Doped Barium Titanate ($BaTiO_3$) Synthesized through Molten Salt Method as Promising Dielectric Material

RICHA TOMAR[1,*], KARAN SURANA[2], PANKAJ GUPTA[1] and N.B. SINGH[1,3]

[1]Department of Chemistry and Biochemistry, Sharda University, Greater Noida-201306, India
[2]Material Research Laboratory, School of Basic Sciences &Research, Sharda University, Greater Noida-201306, India
[3]Research and Development Cell, Sharda University, Greater Noida-201306, India

*Corresponding author: E-mail: richa.tomar@sharda.ac.in

Received: 30 April 2021; *Accepted*: 5 August 2021; *Published online*: 20 August 2021; AJC-20486

Tin doped barium titanate ($BaTiO_3$) was prepared through NaCl-KCl eutectic melt at 800 ºC. The synthesized materials were well characterized using powder-X-ray diffraction (PXRD) and FESEM-EDX spectroscopy. Cubic structure was observed in the PXRD pattern of tin doped sample. The crystallite size of tin doped barium titanate nanoparticles was found to be around 17 nm. Nanorods and aggregated nanocubes like structure were observed in the FESEM images and elemental ratio of doped ions was confirmed by energy dispersive X-ray spectrum (EDX). Electrical properties observed for the synthesized material were found better than those reported in the literature prepared by other methods. The dielectric constant and dielectric loss were measured in the temperature range of 100-400 K and the frequencies varying from 10 kHz to 10,000 kHz. The tin doped barium titanate showed rod type morphology with an unprecedented high dielectric constant of ~17,500 at 10 Hz. Dielectric constant values decreased with increasing frequency. The change in dielectric constant with frequency was well explained by Maxwell-Wanger polarization effect. The impedance and ionic transference number (t_{ion}) were also measured.

Keywords: Eutectic melt, Molten salt, Barium titanate, Dielectric constant, Impedance analysis.

INTRODUCTION

Barium titanate ($BaTiO_3$) is a versatile material known since long for its ABO_3 type structure and properties. Due to its exceptionally high dielectric, ferroelectric and piezoelectric properties, barium titanate is the most studied ceramic substance [1]. Depending on the temperature, barium titanate exists in four polymorphic phases: rhombohedral (T < -90 ºC), orthorhombic (-90 ºC < T < 5 ºC), tetragonal (5 ºC < T < 120 ºC) and cubic (T > 120 ºC) [2]. The crystalline forms of barium titanate are cubic, tetragonal, and hexagonal. Because of its excellent ferroelectric, piezoelectric and thermoelectric capabilities, the tetragonal polymorph is the most commonly used [3].

$BaTiO_3$ is cubic above 120 ºC (and up to 1400 ºC). Doped barium titanate is a well-studied and hot area of research due to high impact of dopant on diffusion and its dielectric, ferroelectric, piezoelectric and magnetic properties. Tin doped $BaTiO_3$ shows three times higher permittivity in comparison to undoped $BaTiO_3$ [4]. The literature survey has also revealed multiple times enhancement of photoluminescent properties of tin doped $BaTiO_3$ [5].The enhancement is due to the stabilization of the defects created by Ti^{4+} upon doping with Sn^{2+} ions in $BaTiO_3$ nanoparticles. However, it is interesting to note that with tin doping, the tetragonal to cubic transition shifts to lower temperature and the remaining transition temperatures shift to higher temperature and therefore, offer the possibility of tuning the transition temperature close to room temperature. From X-ray diffraction study, it was observed that tin doped $BaTiO_3$ exhibited tetragonal structure (*P4mm* space group) for less than 5% tin doping and cubic structure (*Pm3m* space group) for more than 10% tin doping [6]. The Ca^{2+} doped $BaTiO_3$ leading to the formation of $Ba_{1-x}Ca_xTiO_3$ (BCT) solid solutions acted as a good substitute of lead-free ferroelectric material [7].

$BaTiO_3$ has been synthesized in number of ways such as solid-state route, solution-based method, microwave, hydro-

thermal reaction route and sol gel route [4,8-15]. Researchers are always keen to produce the material at low temperature with good yield. The most commonly used synthetic route is the solid state method but it has the limitation of high temperature requirement, typically 1100 to 1400 ºC. Sintering at high temperature leads to reduction in particle size, which restricts the utility of the materials for use in electronic industry. This mandates the need of lower synthesis temperature leading to homogeneous structure. A number of low temperature methods like hydrothermal method, spray pyrolysis, sol-gel processing, a microemulsion processing, microwave heating are being used for the synthesis of $BaTiO_3$, but they have their own disadvantages too [3]. The microwave hydrothermal method helps in the synthesis of required product at relatively low temperature but a slight variation in synthesis conditions can lead to change in the particle size. Moreover, with this the obtained $BaTiO_3$ powder remains in paraelectric cubic phase which requires additional energy in the form of heat to allow its transformation into tetragonal phase to obtain good ferroelectric properties. However, the additional heating leads to aggregation of the ultra-fine powder.

Spray pyrolysis is another method for producing $BaTiO_3$ nanoparticles with a tetragonal phase by combining metal nitrates as an oxidant and carbohydrazide as a fuel source with a 1:1 molar ratio. Spray pyrolysis can result in the formation of a secondary phase as well as hollow particles. The second phase is thought to be caused by chemical segregation during precipitation [16]. The sol-gel method is also commonly used wet-chemical synthesis method for creating glassy and ceramic materials. The sol (or solution) gradually progresses towards the creation of a gel-like network containing both a liquid and a solid phase. The gel forms at a temperature of 60-100 ºC but the desired product is formed after the calcination at 1000-1200 ºC, which makes it a high temperature synthesis. The precursors are comparatively expensive and shows low production rate [17].

The synthesis through molten salt method is a cost effective and simple approach for obtaining single phase chemically pure crystalline powder at low temperature. The reaction environment ensures quick and easy dispersion, rearrangement and diffusion of the raw materials. The minimization of interface and surface energies among the constituent material and the salt gives a way for the synthesis of the desired product. A significant part of this synthesis technique is the high aqueous solvency of the salts, which permits their simple evacuation on completion of the reaction. Dispersive $BaTiO_3$ nanoparticles have been prepared by molten salt method using NaCl-KCl eutectic melt [18]. Recently, a comprehensive review on the synthesis of metal oxide nanomaterials through molten salt has been published and this review demonstrates molten salt synthesis route as the better approach to synthesize materials at lower temperature [19]. To the best of our knowledge, the synthesis of tin doped $BaTiO_3$ through molten salt is not yet reported. In this article, tin doped $BaTiO_3$ has been prepared through NaCl-KCl eutectic melt using molten salt synthesis route and this is an attempt to synthesize the material at the lower temperature and their electrical properties were studied.

EXPERIMENTAL

Materials: For the synthesis of Sn doped barium titanate (Sn-$BaTiO_3$), $BaCO_3$ (≥99 % Sigma-Aldrich, USA), TiO_2 (Fisher-Scientific) and $SnCl_2{\cdot}2H_2O$ (Sigma-Aldrich, 99.9%) were used as the precursors. NaCl (99.5% Thomas-Baker, India) and KCl (99.5% Qualigens, India) salts were used to provide the molten medium.

Synthesis of tin doped barium titanate: The molten salt synthesis route was used for preparing Sn doped $BaTiO_3$. Prior to usage of precursors, the oxides and carbonates were dried at 400 ºC and then weighed in the stoichiometric proportion. The eutectic mixture of NaCl and KCl (1:1 molar ratio) with melting point 665 ºC was prepared. The reactants along with 20 wt.% $SnCl_2{\cdot}2H_2O$ and eutectic mixture were used in the ratio of 1:2, mixed uniformly by grinding for 0.5 h with the help of agate mortar and pestle. The powder was then transferred to alumina crucible and heated at 800 ºC (3 h) where Sn-$BaTiO_3$ was formed. After this, the reaction system was cooled and washed several times to remove chloride ions.

Characterization: Powder X-ray diffraction studies were carried out with the help of Rigaku Ultima IV X-ray diffractometer using CuK_α radiation (45 kV and 40 mA) at a speed of 2 º/min in the range 10º-60º. Using Scherrer's formula, the crystallite sizes (t_c) of the material were calculated from the peaks of XRD patterns.

$$t_c = \frac{K\lambda}{\beta\cos\theta}$$

where, K is the shape coefficient (value between 0.9 and 1.0), λ is the wave length, β is the full-width at half-maximum and θ is the diffraction angle

Field emission scanning electron microscopy was used for morphological studies (FEI Nova Nano FESEM 450). Dielectric constant and electrical conductivity were measured as a function of frequency (10-10,000 kHz) and temperature (RT-400 ºC). The measurements were done using Agilent E4980A LCR meter on a pellet (thickness was 0.14/0.18 cm with 0.08 cm diameter) made by using the hydraulic press under a pressure of 2000 psi for 60 s. A micrometer was used to measure the samples' thickness and diameter. Silver paste was applied on both surfaces of the samples, which were then heat-treated at 800 ºC for 30 min to guarantee electrode contact with the ceramic surface. The CHI 604D electrochemical workstation was used to study the variation of dielectric constant with frequency (5 Hz to 800,000 Hz) at room temperature. The pellets were coated with silver paste and placed in the sample holder. AC impedance mode was selected with an operating voltage of 0.5 V, frequency range of 1 MHz to 100 MHz and amplitude of 50 mV. Ionic transference number (t_{ion}) of the sintered Sn doped $BaTiO_3$ was carried out by bulk electrolysis with coulometric technique at an operating potential of 0.5 V for a duration of 2300 s.

RESULTS AND DISCUSSION

Structural analysis: PXRD pattern of sintered crushed powder of tin doped $BaTiO_3$ is given in Fig. 1. For comparison, the PXRD pattern of pure $BaTiO_3$ (synthesized *via* sol gel

route) is also given in Fig. 1 [4]. Due to doping of Sn in $BaTiO_3$, the peaks slightly shifted towards lower angle as compared to that of pure $BaTiO_3$. The shifting of peaks are well observed in the X-ray pattern of samples synthesized from molten salt route and flux route. The shift of peaks towards lower 2θ value is due to increased lattice parameters. It appears that some of the Sn^{2+} got oxidized to Sn^{4+} and replaced Ti^{4+}, leading to increased lattice dimension resulting in shifting of peaks.

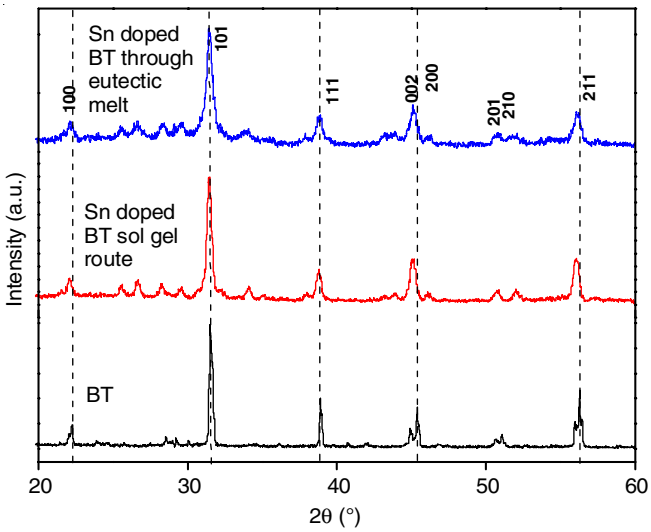

Fig. 1. Powder X-ray diffraction pattern of pure $BaTiO_3$ (BT) and Sn doped $BaTiO_3$ synthesized through eutectic melt and sol gel route

The diffraction patterns are quite similar to the JCPDS file No. 00-005-0626, which represents the tetragonal structure of $BaTiO_3$, but the absence of the (002) and (210) peaks indicate the presence of cubic structure in Sn doped $BaTiO_3$.

A probable mechanism for the formation of Sn doped $BaTiO_3$ through NaCl-KCl eutectic melt is shown in Fig. 2. The molten salt synthesis is a method of preparation of ceramic powders by the use of molten salt as a medium of propagation of reaction. The molten salt's melting point must be lower than the temperature at which the product is formed. Furthermore, once the reaction is complete, the salt should be easily removed, and there should be no reaction between the salt and the product generated or constituent oxides. The chlorides and precursors were weighed and the powders were given a temperature treatment above the melting temperature of the salt after mixing and grinding. As the temperature rises, the chlorides melt, providing a homogeneous medium for the production and the development of product nuclei during the reaction. The reacting material (salts and product nuclei) is cooled at room temperature before being washed with water to remove the salts. The solid particles nucleate uniformly in the liquid phase after cooling as shown in Fig. 2. The main roles of molten salt are (i) to increase the reaction rate and lower the reaction temperature; (ii) to increase the degree of homogeneity; (iii) to control the agglomeration of the particles; and (iv) to control particle shape and size.

SEM studies: It can be inferred from Fig. 3a-c that Sn doped $BaTiO_3$ exhibits a compact arrangement of nanorods and aggregated nanocubes forming sheet like structure at some places with smooth and clean surfaces. The volume ratio in 1D nanorods was decreased, and some sheet like structure appeared probably due to increased reaction time of 8 h. It is reported that longer reaction time in molten salt synthesis route promotes the formation of aggregated large plate like structures at the expense of rod like structure [20]. The average particle size was 65 nm. When Sn is substituted for Ba or Ti, it causes point flaws and distortion, resulting in strain energy. Reduced strain energy increases the formation energy of oxygen vacancies and the grain boundary diffusion coefficient to some extent. Increased defects improve the mass transport process, resulting in increased diffusion and particles of varying form and size, because of few agglomerated particles of different shapes.

The EDX spectrum confirmed the presence of Sn and Ba (Fig. 4). Along with main elements, the peak of Au is also visible in EDX spectrum although Au was not present in the main composition. Actually the Au coating is used to make the surface conducting while taking the EDX spectrum.

Electrical properties

Dielectric constant measurements: The dielectric constant is a measure of the amount of electric potential energy stored in a specific volume of material under the action of an electric field in the form of induced polarization. It is calculated as the

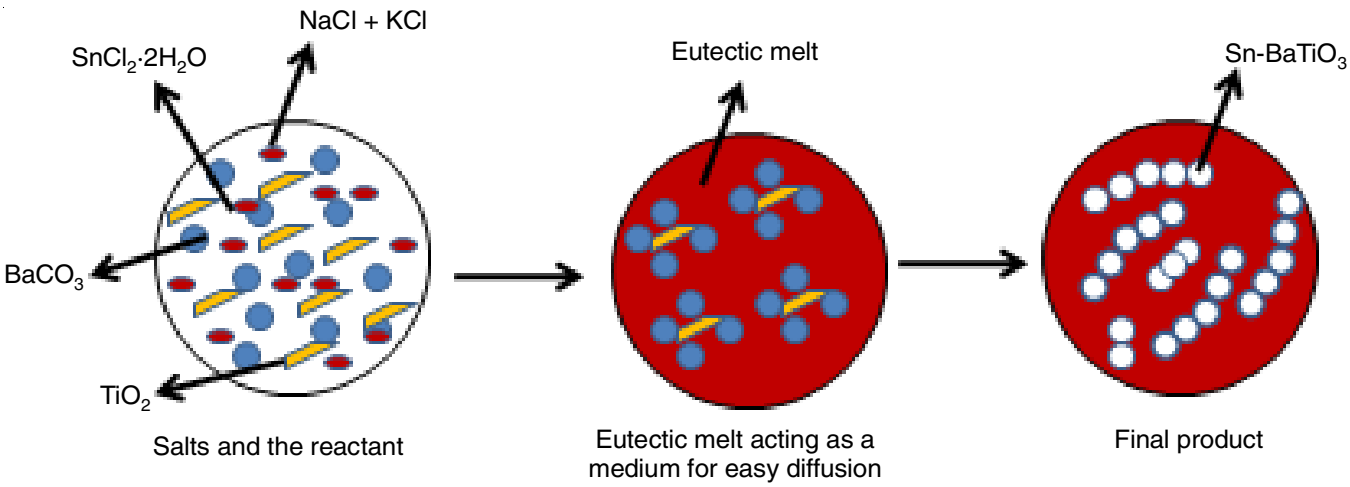

Fig. 2. Probable mechanism of formation of Sn doped $BaTiO_3$

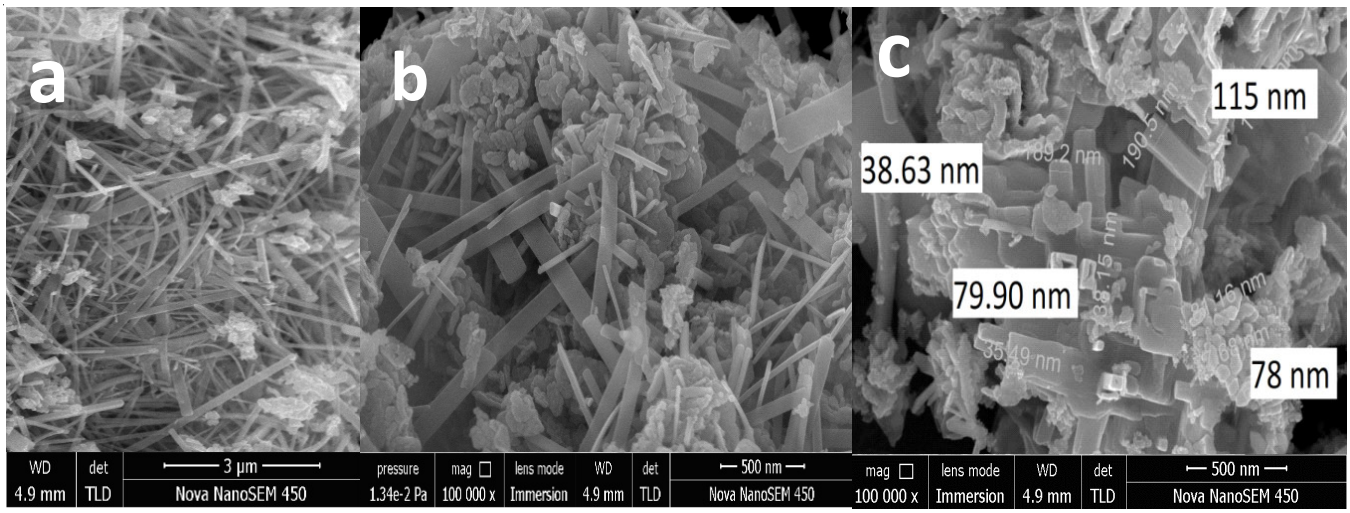

Fig. 3. FESEM images (at different magnifications) of Sn doped $BaTiO_3$ (nanorods) synthesized *via* flux route at 800 °C

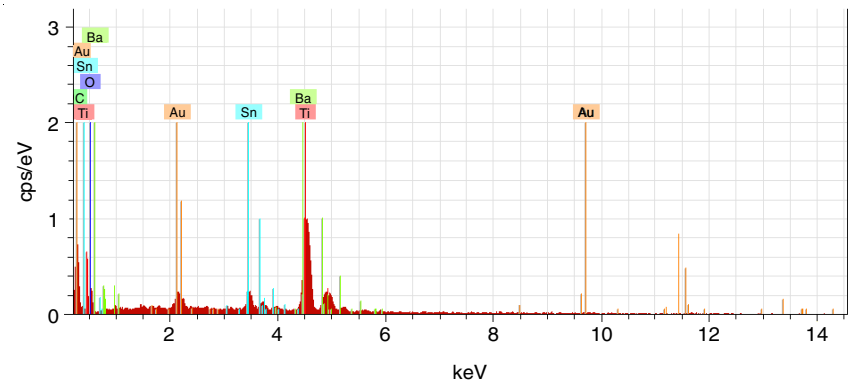

EIAN series	unn.C (wt.%)	norm.C (wt.%)	Atom.C (at.%)
Ti 22 K-series	30.03	37.44	22.30
C 6 K-series	16.45	20.52	48.72
O 8 K-series	10.46	13.04	23.24
Ba 56 L-series	9.98	12.45	2.59
Au 79 M-series	6.93	8.64	1.25
Sn 50 L-series	6.35	7.92	1.90
Total	80.20	100.00	100.00

Fig. 4. Energy dispersive X-ray spectrum and wt% of different elements present in Sn doped $BaTiO_3$ (nanorods) synthesized using molten salt synthesis route

ratio of the material's dielectric permittivity to that of a vacuum or dry air. The dielectric constants of the sintered samples were obtained by using eqns. 1-3 as follows:

$$\varepsilon = \frac{C}{C_o} \tag{1}$$

$$C_o = \frac{\varepsilon_o A}{d} \tag{2}$$

$$\varepsilon = \frac{\varepsilon_o A}{dC_o} \tag{3}$$

where, C = capacitance with the dielectric material in between the electric plates, C_o = capacitance with vacuum in between the electric plates, ε = permittivity of the material, ε_o = permittivity of free space (8.854×10^{12} Farads/m), A = area of pellet (m^2), d = thickness of pellet or distance between the plates (m).

Variation of dielectric constant (ε) and dielectric loss (tan δ) of Sn-$BaTiO_3$ in the temperature range of 100-400 K and frequency range of 10-10,000 kHz are shown in Fig. 5. The values of dielectric constant (16581) and dielectric loss (3797) were found maximum at 10 kHz and 340 K, respectively. The higher dielectric constant could be due to the space charge polarization arising from oxygen vacancies [21]. When Sn-$BaTiO_3$ sintered, the following reaction firstly occurs in the tin doped $BaTiO_3$ ceramic as:

$$2Ti^{3+} + Sn^{4+} \longrightarrow 2Ti^{4+} + Sn^{2+}$$

In this reaction, Ti^{3+} is oxidized to Ti^{4+} since standard oxidation-reduction potential of Sn^{2+}/Sn^{4+} couple (0.15 V) is higher than the Ti^{4+}/Ti^{3+} (0.10V), hence the Sn-$BaTiO_3$ has better crystallinity. Besides, Sn^{4+} will be reduced to Sn^{2+} to act as an acceptor doping, which require oxygen vacancies for charge compensation. The immobile defect complex ($Sn''_{Ti} - V_o^{\bullet\bullet}$) could suppress the oxygen vacancy migration and improve the insulator resistance of $BaTiO_3$ sintered. Fig. 6 shows the plot of dielectric constant with frequency and for comparison the dielectric constant values obtained for the samples synthesized through sol gel method were also plotted. The inset figure shows the expanded lower frequency region. The Sn-$BaTiO_3$ synthesized *via* eutectic melt shows an unprecedented high dielectric constant of ~17,500 at 10 Hz, while at the same frequency the sol-gel sample has the dielectric constant of ~7,500. $BaTiO_3$ nanorods using molten salt synthesis route was reported to have a very low dielectric constant of around 700 at 10 Hz [15]. The dielectric constant for Sn doped $Ba_{1-x}Ca_xTiO_3$ ($x = 0.13$) reported in the literature was around 1700 [9]. Ding *et al*. [22]

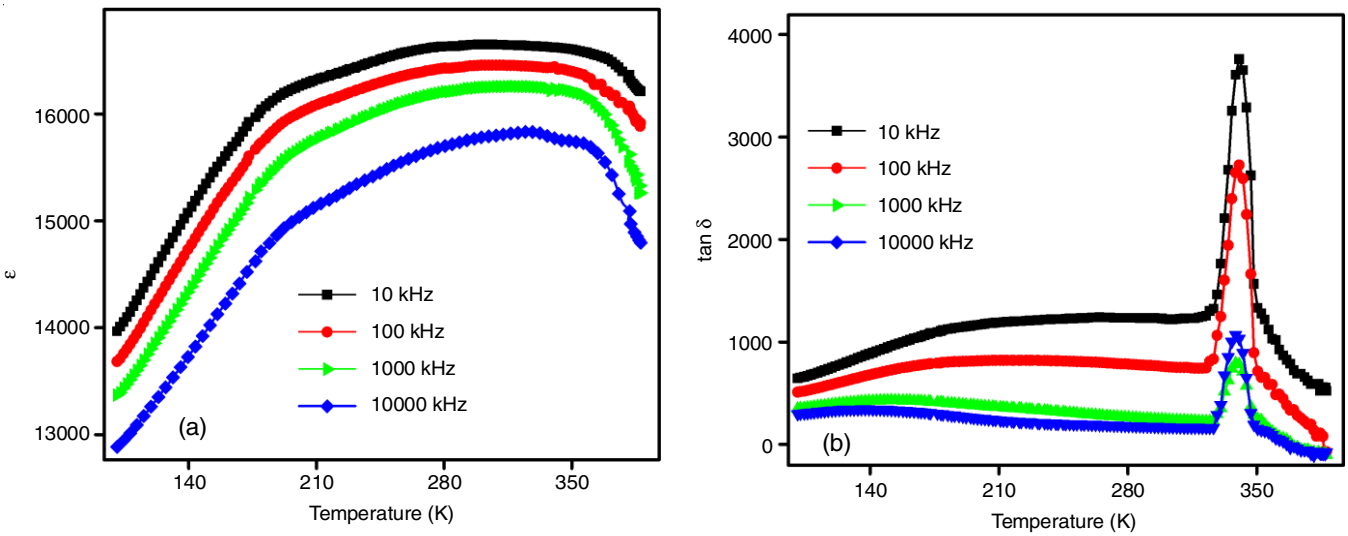

Fig. 5. Variation of dielectric constant and dielectric loss of Sn-BT with temperature

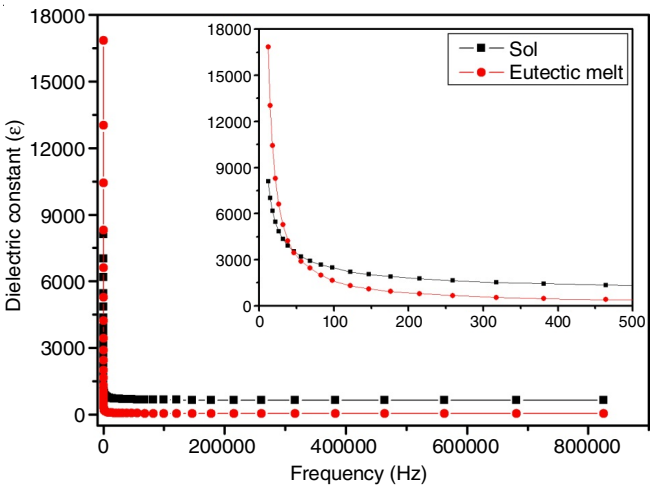

Fig. 6. Comparative plot of dielectric constant *vs.* frequency for the Sn doped $BaTiO_3$ samples synthesized through sol gel and molten salt method. (Inset) Expanded initial frequency region

studied the dielectric properties of $BaTi_{1-x}Sn_xO_3$ synthesized through solid state method at 1200 ºC, the obtained dielectric constant was around 9500 for 10% insertion of Sn at place of Ti. Ansari & Sreenivas [23] observed the value of 6300 for 20% Sn doped $BaTiO_3$ (solid state method) at 1100 ºC. A dielectric constant value of 1201 was obtained for $Ba_{0.8}Sn_{0.2}TiO_3$ (microwave assisted solvothermal synthesis) at 1100 ºC [20]. The results showed that the molten salt route for synthesis of Sn-$BaTiO_3$ is an exceptionally useful method, if played well with temperature and time of reaction.

From Figs. 5 and 6, it can clearly observed that from 10 Hz to 10 kHz, the dielectric constant value remains almost constant (around 17,000) and after that there is a decreasing trend. At low frequency, it is possible that the dipole follows the dielectric field and align in the direction of applied field, resulting in increase of dielectric constant (ε′). But at higher frequencies, the relaxation time required by the dipole to align in the direction of applied field would decrease leading to lower dielectric constant and dielectric loss [21]. The materials with high dielectric constant can be used in energy storage devices like capacitors. These dielectric materials with high dielectric constant also act as good ferroelectric materials as they exhibit spontaneous charge polarization that can be reversed by changing the direction of the electric field.

Impedance analysis: The Nyquist plot of Sn doped $BaTiO_3$ sintered at 800 ºC is shown in Fig. 7. The semi-circular arcs are due to the parallel combination of capacitance and resistance. Nyquist plot usually comprises of three semi-circles depending on the electrical properties of the material. The first semi-circle corresponding to higher frequency represents the resistance of grains, while the second semi-circle corresponds to the resistance of bulk material grain and grain boundaries [24] and the third semi-circle observed is due to the electrode effect [25]. The semi-circular arcs of Cole-Cole plot (Fig. 7) represent the contribution of grain and grain boundaries for the overall electrical properties. The first semi-circular arc if extended will take the shape of a perfect semi-circle whose center will lie at the Z′-axis, which is the characteristic behaviour of the ideal Debye type relaxation. The appearance of third semi-circle in the Nyquist plot suggests some very small contributions of electrode-material interface to impedance.

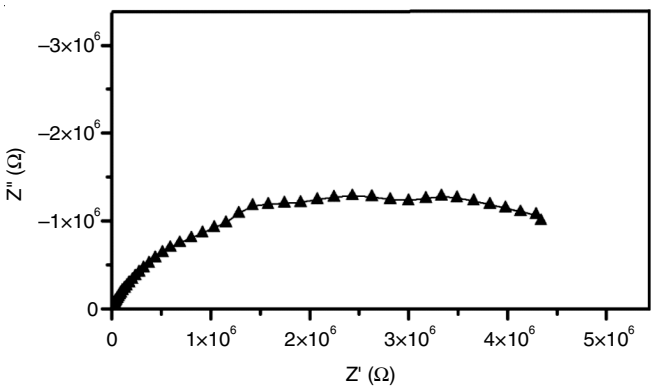

Fig. 7. Cole-Cole plot of sintered Sn doped BT sample

In order to understand the type of electrical conduction occurring in the sample, t_{ion} measurement was made using eqn. 4:

$$t_{ion} = \frac{I_{initial} - I_{final}}{I_{initial}} \quad (4)$$

where, $I_{initial}$ and I_{final} are the initial and final currents, respectively [26].

The obtained current conduction pattern is shown in Fig. 8, where an initial steep decrement is followed by a slow and slightly irregular curve. Upon estimating the $I_{initial}$ and I_{final} values, the calculated t_{ion} value was found to be 0.55. This clearly suggests that the Sn-$BaTiO_3$ sample possessed mixed ionic and electronic conductivity with slight dominance of ionic conductivity. Since the experimental process suggests the substitution of Sn^{4+} ions in place of Ti^{4+}, thereby rendering the Ti^{4+} ions out of the lattice, hence the dominant species for the ionic conduction would be Ti. The electronic conduction would then take place due to the hopping mechanism of the electrons.

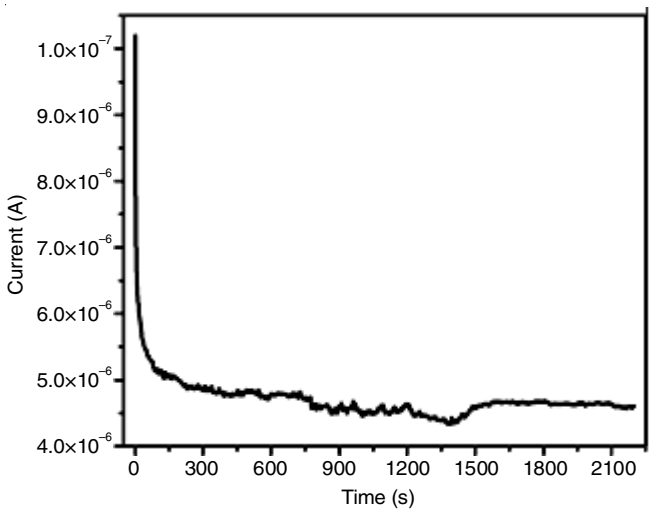

Fig. 8. Ionic transference number (t_{ion}) of Sn doped $BaTiO_3$

Conclusion

The molten salt route is found to be a better approach in comparison to other known routes for the synthesis of Sn doped $BaTiO_3$, primarily because the molten salt route has enabled the synthesis at lower temperature (800 ºC). Homogeneity, control of agglomeration and control of particle size were also seen in the molten salt method. The powder X-ray diffraction patterns showed the cubic structure after incorporation of tin in barium titanate with slightly shifting of PXRD peaks at lower angle due to the replacement of bigger ion (Ti^{4+}) with smaller ion (Sn^{4+}) without any secondary phase. Nano rods type morphology was observed in the FESEM images and EDX spectra confirmed the elemental ratio of ions. High dielectric constant of ~17,500 at 10 Hz was observed at low frequency value, which is higher in comparison to the highest reported value of 13,718 synthesized *via* solid state route [21]. The higher value of dielectric constant was only observed at low frequency, while dielectric value started decreasing with increasing frequency. Mechanism of variation of dielectric constant with frequency has been explained by Maxwell-Wanger theory. The Cole-Cole plot showed that upon sintering, the impedance of the samples improves significantly because of orientation of the crystals, resulting in lowering of the path resistance of the sample thereby improving the overall impedance characteristics of the material.

ACKNOWLEDGEMENTS

The authors are thankful to Sharda University for providing the seed fund and to the Instrumentation Center, Jamia Millia Islamia University, New Delhi, India for performing the characterization of the samples.

CONFLICT OF INTEREST

The authors declare that there is no conflict of interests regarding the publication of this article.

REFERENCES

1. B.G. Baraskar, P.S. Kadhane, T.C. Darvade, A.R. James and R.C. Kamble, Ferroelectrics and their Applications, IntechOpen, Chap. 7, p. 113 (2018).
2. S. Nayak, B. Sahoo, T.K. Chaki and D. Khastgir, *RSC Adv.*, **4**, 1212 (2014); https://doi.org/10.1039/C3RA44815K
3. K.I. Osman, Ph.D. Thesis, Synthesis and Characterization of $BaTiO_3$ Ferroelectric Material, Faculty of Engineering, Cairo University, Egypt (2011).
4. R. Tomar, R. Pandey, N.B. Singh, M.K. Gupta and P. Gupta, *SN Appl. Sci.*, **2**, 226 (2020); https://doi.org/10.1007/s42452-020-2017-8
5. R. Tomar, R. Prajapati, S. Verma and N. Rana, *Mater. Today Proc.*, **34**, 608 (2021); https://doi.org/10.1016/j.matpr.2020.01.543
6. S.K. Upadhyay, V.R. Reddy, P. Bag, R. Rawat, S.M. Gupta and A. Gupta, *Appl. Phys. Lett.*, **105**, 112907 (2014); https://doi.org/10.1063/1.4896044
7. A. Taibi, S. Chaguetmi, A. Louaer, A. Layachi and H. Satha, *Thermochim. Acta*, **680**, 178356 (2019); https://doi.org/10.1016/j.tca.2019.178356
8. Y. Hou, L. Yang, X. Qian, T. Zhang and Q.M. Zhang, *Phil. Trans. R. Soc. A*, **374**, 20160055 (2016); https://doi.org/10.1098/rsta.2016.0055
9. S. Suzuki, T. Takeda, A. Ando and H. Takagi, *Appl. Phys. Lett.*, **96**, 132903 (2010); https://doi.org/10.1063/1.3367733
10. S. Suzuki, T. Takeda, A. Ando, T. Oyama, N. Wada, H. Niimi and H. Takagi, *Jpn. J. Appl. Phys.*, **49**, 09MC04 (2010); https://doi.org/10.1143/JJAP.49.09MC04
11. K.C. Singh, A.K. Nath, R. Laishram and O.P. Thakur, *J. Alloys Compd.*, **509**, 2597 (2011); https://doi.org/10.1016/j.jallcom.2010.11.106
12. W. Liu, J. Wang, X. Ke and S. Li, *J. Alloys Compd.*, **712**, 1 (2017); https://doi.org/10.1016/j.jallcom.2017.04.013
13. M.J. Ansaree and S. Upadhyay, *Emerg. Mater. Res.*, **6**, 21 (2017); https://doi.org/10.1680/jemmr.16.00013
14. J. Wang, S. Jiang, D. Jiang, T. Wang and H. Yao, *Ceram. Int.*, **39**, 3657 (2013); https://doi.org/10.1016/j.ceramint.2012.10.195
15. Y. Xie, S. Yin, T. Hashimoto, H. Kimura and T. Sato, *J. Mater. Sci.*, **44**, 4834 (2009); https://doi.org/10.1007/s10853-009-3737-8
16. B.G. Jeyaprakash, R.A. Kumar, K. Kesavan and A. Amalarani, *Am. J. Sci.*, **6**, 22 (2010).
17. A. Kumar, N. Yadav, M. Bhatt, N.K. Mishra, P. Chaudhary and R. Singh, *Res. J. Chem. Sci.*, **5**, 98 (2015).
18. Y. Zhang, L. Wang and D. Xue, *Powder Technol.*, **217**, 629 (2012); https://doi.org/10.1016/j.powtec.2011.11.043

19. S.K. Gupta and Y. Mao, *Prog. Mater. Sci.*, **117**, 100734 (2021); https://doi.org/10.1016/j.pmatsci.2020.100734
20. P. Xue, H. Wu, W. Xia, Z. Pei, Y. Lu and X. Zhu, *J. Am. Ceram. Soc.*, **102**, 2325 (2019); https://doi.org/10.1111/jace.16123
21. J. Livage, M. Henry and C. Sanchez, *Prog. Solid State Chem.*, **18**, 259 (1988); https://doi.org/10.1016/0079-6786(88)90005-2
22. S.-W. Ding, J. Chai and C.-Y. Feng, *Mater. Lett.*, **60**, 3241 (2006); https://doi.org/10.1016/j.matlet.2006.02.087
23. M.A. Ansari and K. Sreenivas, *Ceram. Int.*, **45**, 20738 (2019); https://doi.org/10.1016/j.ceramint.2019.07.058
24. H. Inaba, *J. Mater. Sci.*, **32**, 1867 (1997); https://doi.org/10.1023/A:1018561024682
25. M.H. Abdullah and A.N. Yusoff, *J. Mater. Sci.*, **32**, 5817 (1997); https://doi.org/10.1023/A:1018690322459
26. K. Surana, P.K. Singh, B. Bhattacharya, C.S. Verma and R.M. Mehra, *Ceram. Int.*, **41**, 5093 (2015); https://doi.org/10.1016/j.ceramint.2014.12.080